Supplementary Information for

The Behaviors of Ferro-Magnetic Nano-Particles In and Around Blood Vessels under Applied Magnetic Fields

A.Nacev[*14], C.Beni[2], O.Bruno[2], B.Shapiro[134]

[*]Corresponding author, email: alek@umd.edu ; [1]Fischell Department of Bioengineering; [2]Applied and Computational Mathematics, California Institute of Technology; [3]Institute for Systems Research; and [4]University of Maryland at College Park.

S1. Non-Dimensionalizing the Governing Equations

In a model with dimensional parameters, like equation (10), the numerical parameter values used depend on the chosen units (meters versus millimeters), there are typically multiple parameters associated with each phenomena (with diffusion, convection, and magnetic drift), and their effects are coupled together (for example, changing the particle radius changes both the diffusion coefficient D and the magnetic drift coefficient k). Non-dimensionalizing (i.e. normalizing) the model reduces the number of parameters to those that are actually independent [76]. The resulting non-dimensional numbers capture the ratio between competing physical effects; they remain the same even if a different system of units is chosen; and they are uncoupled in the sense that each non-dimensional number is the ratio between two competing effects and is independent from parameters that make up any third effect (e.g. the Renkin number is a ratio of diffusion in tissue versus in blood and does not depend on particle size).

As described in the main text, for our idealized blood vessel system, nano-particle behavior is uniquely determined by three non-dimensional numbers: the magnetic-Richardson number, the Renkin reduced diffusion coefficient, and the mass Péclet number. If we consider two situations A and B in which the blood vessel width, particle size, and magnetic field strength differ dramatically, but these two situations share the same three non-dimensional Richardson, Renkin, and Péclet numbers, then these two different situations will exhibit identical behavior because they will both have exactly the same balance of magnetic, diffusion, and convection phenomena.

We now formally derive the non-dimensional form of our model (equations (13), (14), and (15)) from the dimensional form. Repeating equation (10) for clarity

$$\text{(S1)} \quad \frac{\partial C}{\partial t} = -\nabla \cdot \left[- D_{Tot} \nabla C + C \vec{V}_B + C \vec{V}_R \right]$$

let $\hat{x} = x / d_B$, $\hat{y} = y / d_B$, $\hat{C} = C / C_o$, $\hat{\vec{V}}_B = \vec{V}_B / V_{B\max}$, $\hat{\vec{V}}_R = \vec{V}_R / V_{B\max}$ so each non-dimensional variable (hatted) is the dimensional variable divided by a characteristic quantity. Here d_B, C_o, and $V_{B\max}$ are the characteristic length (the width of the blood vessel), characteristic concentration (the inlet magnetic particle concentration), and the characteristic velocity (the maximum centerline velocity in the blood vessel). Using these three characteristic quantities, it is further possible to consistently define all other needed non-

dimensional variables and derivative operators as $\hat{t} = t\,(V_{B\max}/d_B) = t/t_o$, $\partial\hat{t}/\partial t = 1/t_o$ and $\nabla = \partial/\partial(x) = \partial/\partial(d_B\hat{x}) = \hat{\nabla}/d_B$.

Table S1 summarizes the non-dimensional transformations for all variables. The five essential dimensional variables (those variables that are bolded in Table 1 in the main text) reduce down to just two non-dimensional numbers, as predicted by the classical theorem of non-dimensional analysis: the Buckingham Pi Theorem [76]. These two non-dimensional numbers are the magnetic-Richardson number and the mass Péclet number. The third non-dimensional number considered in the paper, the Renkin reduced diffusion coefficient of the endothelial membrane or the tissue, is required because diffusion in the endothelium or the tissue differs from diffusion in the blood.

Table S1: The non-dimensionalized variables.

Parameter	**Dimensional Symbol [and units]**	**Non-Dimensional Version**	**Characteristic Quantity Used for Non-Dimensionalization**
Particle Radius	a [m]	$\hat{a} = a/d_B$	d_B the average width of the blood vessel, e.g. d_B = 0.03 mm for an arteriole
X Length	x [m]	$\hat{x} = x/d_B$	
Y Length	y [m]	$\hat{y} = y/d_B$	
Velocity	$\vec{V}$ [m/s]	$\hat{\vec{V}} = \vec{V}/V_{B\max}$	$V_{B\max}$ the maximum centerline blood velocity, e.g. $V_{B\max}$ = 1 cm/s for an arteriole
Concentration	C [mol/m^3]	$\hat{C} = C/C_o$	C_o the inlet concentration, e.g. C_o = 2 to 4 mol/m^3
Time	t [s]	$\hat{t} = t\dfrac{V_{B\max}}{d_B} = \dfrac{t}{t_o}$	Non-dimensionalized by the composite quantity $t_o = d_B/V_{B\max}$
Diffusion Coefficient	D_{Tot} [m^2/s]	$\hat{D}_{Tot} = D_{Tot}\dfrac{t_o}{d_B{}^2} = \dfrac{D_{Tot}}{d_B V_{B\max}}$	Non-dimensionalized by the composite quantity $d_B V_{B\max}$

Substituting the non-dimensional variable (or derivative operator) multiplied by the constant characteristic quantity for each dimensional variable (or operator) rewrites equation (S1) as

$$\text{(S2)}\quad \frac{\partial(C_o\hat{C})}{\partial\hat{t}}\frac{\partial\hat{t}}{\partial t} = -\frac{\hat{\nabla}}{d_B}\cdot\left[-D_{Tot}\frac{\hat{\nabla}(C_o\hat{C})}{d_B} + (C_o\hat{C})\left(V_{B\max}\hat{\vec{V}}_B + V_{B\max}\hat{\vec{V}}_R\right)\right]$$

$$\frac{C_o}{t_o}\frac{\partial\hat{C}}{\partial\hat{t}} = -\frac{1}{d_B}\hat{\nabla}\cdot\left[-D_{Tot}\frac{C_o}{d_B}\hat{\nabla}\hat{C} + C_oV_{B\max}\left(\hat{\vec{V}}_B + \hat{\vec{V}}_R\right)\hat{C}\right].$$

Multiplying both sides by t_o / C_o

$$\text{(S3)}\quad \frac{\partial\hat{C}}{\partial\hat{t}} = -\frac{t_o}{d_BC_o}\hat{\nabla}\cdot\left[-D_{Tot}\frac{C_o}{d_B}\hat{\nabla}\hat{C} + C_oV_{B\max}\left(\hat{\vec{V}}_B + \hat{\vec{V}}_R\right)\hat{C}\right].$$

Canceling and grouping terms, and recalling that t_o is defined to be $d_B / V_{B\max}$ gives

$$\text{(S4)}\quad \frac{\partial\hat{C}}{\partial\hat{t}} = -\hat{\nabla}\cdot\left[\underbrace{-\left[\frac{D_{Tot}}{d_BV_{B\max}}\right]\hat{\nabla}\hat{C}}_{\text{DIFFUSION}} + \underbrace{\left(\hat{\vec{V}}_B + \hat{\vec{V}}_R\right)\hat{C}}_{\text{ADVECTION}}\right].$$

Defining the mass Péclet number to be $\boldsymbol{Pe} = d_BV_{B\max} / D_{Tot}$ and the magnetic Richardson number to be the downward component of the non-dimensional magnetic velocity yields equation (13) in the main text (where the sub-script B has been added to denote nano-particles in blood and the hats have been dropped).

Equations (14) and (15) in the main text are derived in exactly the same way.

S2. Simulation Implementation and Computational Parameters

Below we provide details of both the COMSOL and VMT numerical implementations, as well as a comparison of the two to show that they give the same answer (up to the poorer solution accuracy possible with COMSOL).

S2.1. COMSOL Implementation

S2.1.1. Software Implementation

For implementing the model, the software package COMSOL Multiphysics version 3.4 was chosen initially. This package allowed the geometry specified in Figure 2 to be constructed. Equations (13) to (15) were solved for the entire control volume using the prescribed blood velocity and magnetic velocity (equations (8) and (7)). Simulation times ranged from 15 minutes for the easy cases with $\boldsymbol{Pe} \le 100$, up to 36 hours for $\boldsymbol{Pe} \approx 1000$, and were unsolvable for $\boldsymbol{Pe} \ge 3000$ even when using a high-end quad-core 32 GB RAM computer (a typical 2009 desktop PC or laptop has only 4 GB of RAM available).

S2.1.2. Meshing Parameters

COMSOL computes the solution by using the finite element method; that is by meshing the region and numerically integrating the approximate solution of the PDE at all mesh points until converged [96]. The mesh sizing must be sufficiently small to capture any physics being modeled in the domain. In systems with both

advection and diffusion, the cell Péclet number sets the mesh sizing dependence on the modeled physical phenomena to ensure numerical stability. The cell Péclet number is defined as

$$\text{(S5)} \quad Pe_{cell} = \Psi \, \boldsymbol{Pe} \, dx$$

where dx is the mesh size in any primary coordinate direction. When $Pe_{cell} \leq 2$, the solution is guaranteed to be numerically stable [97]. This requirement for stability demands small mesh elements due to small diffusion coefficients (for a $\boldsymbol{Pe} \approx 1000$ simulation, this requirement translated into 4.7 x 10^7 required mesh points and 80 GB of available memory, either random access or virtual memory). The COMSOL simulations were solved using a computer that contained a quad-core processor. Using COMSOL and this high-end computer we were able to solve cases up to $\boldsymbol{Pe} \leq$ 1300 but higher Péclet number cases remained unsolvable (a $\boldsymbol{Pe} = 1 \times 10^8$ would have required 4.7 x 10^{17} mesh points to ensure numerical stability corresponding to a 2000 Terabytes ≈ 2 × 10^6 Gigabytes of required memory, an infeasible amount).

S2.2. Vessel-Membrane-Tissue (VMT) Solver

The VMT solver provided far more capabilities than COMSOL and was both over 500 times faster than COMSOL and able to solve cases that COMSOL could not. Using the VMT solver we were able to resolve all the needed cases to sufficient accuracy to accurately and unambiguously locate the delineations between our 3 observed behaviors. The VMT solver is comprised of four distinct components used in combination: 1) a graded mesh to adequately resolve thin boundary layers; 2) a change of unknowns that enabled evaluation of steady states in tissue and membrane layers through a highly accelerated time-stepping procedure [55-58]; 3) an on-and-off fluid-freezing methodology that allowed for efficient treatment of the multiple-time scales that exist in the problem; and 4) the Alternating Directions Implicit (ADI) method for solving PDEs [58].

To resolve the thin boundary layer that can form at the interface between the vessel and the endothelial layer, a typical Cartesian mesh was not adequate. Instead, the VMT method used a graded mesh implemented through an exponential change of unknowns of the form

$$\text{(S6)} \quad \xi_j = e^{-\Psi \, \boldsymbol{Pe} \, y_j}, \text{ and}$$

$$\text{(S7)} \quad \begin{aligned} x_i &= (i-1)\,h_x, \quad i = 1,\ldots,N, \quad h_x = 1/(N-1) \\ y_j &= (j-1)\,h_y, \quad j = 1,\ldots,M, \quad h_y = 1/(M-1) \end{aligned}.$$

To numerically resolve advection in the vessel, we began by using a small time step, Δt = 0.1. This presented a problem, however, because diffusion in the membrane and tissue can be small. Therefore using this time step required a long simulation time in order for the concentration to reach steady state. If the time step was taken to be much larger, we risked being unable to resolve ferrofluid advection in the vessel. To overcome this difficulty, we periodically "froze" and "un-froze" the concentration in the blood vessel. Freezing occurred once the concentration in the blood vessel approached steady state allowing for only the concentration in the membrane and tissue to be evolved. Evolution of the concentration in only the membrane and tissue continued until the freezing approximation was no longer accurate, at which time we unfroze the concentration in the blood, and evolved the entire system at a significantly reduced time-step until freezing could be performed again. The process was repeated until steady-state in the complete system was reached.

In order to quickly obtain steady states in the membrane and tissue regions for each frozen vessel concentration, we performed a transformation that allowed us to take advantage of a fast steady-state solver based on selection of adequately chosen, very large time-steps. The required transformation was a change of unknowns

$$C_M(x,y,t) = \omega_M(x,y,t)e^{-\psi y\,\boldsymbol{Pe}/2}$$
$$C_T(x,y,t) = \omega_T(x,y,t)e^{-\psi y\,\boldsymbol{Pe}/2}$$

that eliminated the magnetic term in the PDE for the membrane and tissue, converting the convection diffusion spatial operator to a spatial operator of Helmholtz type

$$\frac{\partial \omega_M}{\partial t} = -\nabla\cdot\mathcal{D}\left[-\frac{1}{\boldsymbol{Pe}}\nabla\omega_M\right] - \frac{\psi^2}{4}\omega_M$$
$$\frac{\partial \omega_T}{\partial t} = -\nabla\cdot\mathcal{D}_T\left[-\frac{1}{\boldsymbol{Pe}}\nabla\omega_T\right] - \frac{\psi^2}{4}\omega_T$$

We then selected time-steps in a form described in [98], that is

$$\Delta t_n = \frac{h_M^2}{b}\left(\frac{b}{a}\right)^{\frac{n+1}{100}},$$

where

$$a = 4\sin^2\left(\frac{\pi\, h_M}{2}\right), \quad b = 4\cos^2\left(\frac{\pi\, h_M}{2}\right),$$

h_M is the step size in the *y*-direction in the membrane, and *n* is the iteration number. This was done in conjunction with freezing the concentration in the vessel to obtain fast convergence.

An essential element of the overall VMT solver was the Alternating Directions Implicit (ADI) methodology first introduced in [55-58]. Based on reducing a given PDE into separate ODEs through the factorization of terms associated with a particular variable, ADI methods require line-by-line solutions of small sets of simultaneous equations. The key feature of these methods is their unconditional stability, thus permitting our VMT solver to avoid the extremely small time-steps imposed for stability by explicit schemes in the presence of small diffusion coefficients and allowing the use of the efficient time-stepping scheme described earlier. The ODEs generated from this method can be solved by using a variety of methods. Because of the rectangular geometry being considered for the VMT solver, a standard Finite Difference approach was used. For general (e.g. curved) domains, another approach is required. The only available methodology that gives rise to unconditionally stable numerics for the Alternating Directions method in general non-rectangular domains is the Fourier Continuation-Alternating Directions (FC-AD) approach introduced in [90]. By solving the ODEs generated in the ADI algorithm through the use of Fourier Continuation methods [99], the FC-AD algorithm has the ability to yield high-order accurate, unconditionally stable solutions in essentially linear time. The FCAD algorithm is currently being implemented for future simulations of flow through more complex vasculature geometries and will be presented in a forthcoming paper, [91].

S2.3. Comparison of COMSOL versus VMT

Up to the accuracy possible in COMSOL, the two numerical methods provide the same answers. Below we show two side-by-side comparisons: one easy case in which the COMSOL solution accuracy is sufficient (here there is a very good match between COMSOL and VMT) and one medium-difficulty case where COMSOL was able to find a solution but the accuracy of VMT is better. For hard (high Péclet number) cases, COMSOL cannot provide a solution and VMT is the only option.

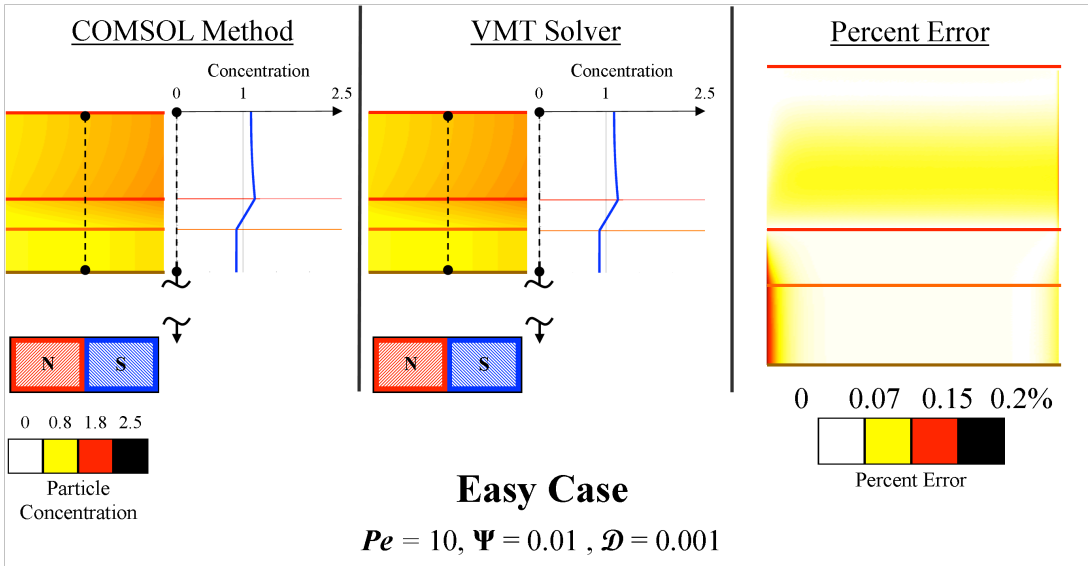

Figure S1: Easy case at a $Pe = 10$, $\Psi = 10^{-2}$, $\mathcal{D} = 10^{-3}$. Cross-sectional magnetic nanoparticle concentration for steady state for both COMSOL and the VMT method. The percent error is calculated by $(C_{Comsol} - C_{VMT})/C_{VMT}$.

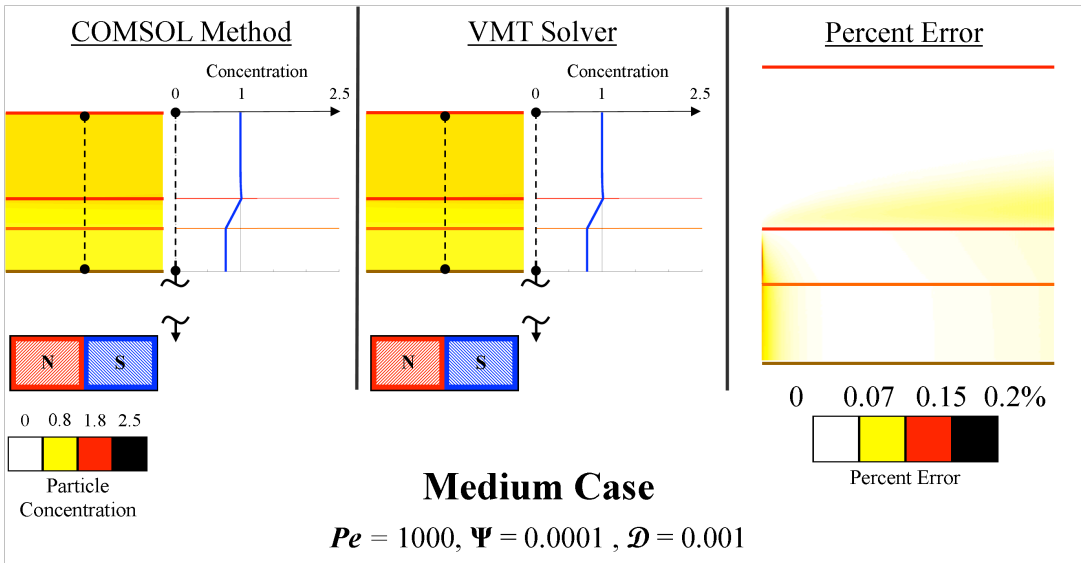

Figure S2: Medium case at a $Pe = 1000$, $\Psi = 10^{-4}$, $\mathcal{D} = 10^{-3}$. Cross-sectional magnetic nanoparticle concentration for steady state for both COMSOL and the VMT method. The percent error is calculated by $(C_{Comsol} - C_{VMT})/C_{VMT}$.

S3. Relaxing the Idealizations: Added Simulation Features

Additional features can be added to relax simulation idealizations. These features sometimes make a quantitative difference to the nano-particle concentration profiles but, with the exception of the skin boundary condition, they do not make a qualitative difference. The three behavioral forms still occur though their delineations can shift moderately depending upon the features added.

S3.1. No Extravasation through Blood Vessel Membrane

First there is a trivial case to consider when the blood vessel will not allow any particles to pass through the membrane into the surrounding tissue: i.e. no extravasation. This case can be modeled by forcing the flux normal to the blood vessel membrane surface to be equal to zero. Figure S3 shows how the two characteristic behaviors (velocity dominated and boundary layer formation) remain in effect in this case. The magnetic dominated behavior, however, which requires particles to move from the blood into the tissue, is no longer possible.

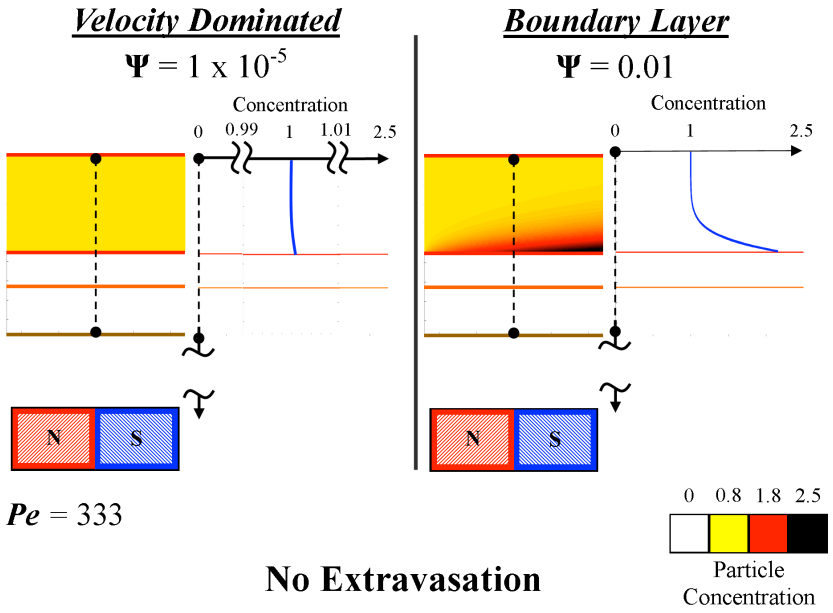

Figure S3: No extravasation through the blood vessel membrane. The characterisitic behaviors still exhibit their defining characteristics within the blood vessel. The magentic dominated case is no longer possible. Instead, when there is no extravasation (e.g. for particles bigger than blood vessel fenestrations) magnetic dominated behavior is replaced by a boundary layer type behavior.

S3.2. Pulsatile Blood Flows

Flow in blood vessels is pulsatile [83, 100-103], its forward velocity increases and decreases as the heart pumps (see Figure 5(a) in [100] of an archetypal peak velocity waveform complied from 3560 cardiac cycles). We now include this blood velocity oscillation and show that it does not qualitatively change the 3 types of behavior we see – we still find a magnetic dominated, velocity dominated, and boundary layer regime.

The waveform associated with high pulsatile cardiac blood flow was used to set the blood velocity in time. A choice of three heart rates was used (a resting heart rate of 1 Hz, 1.5 Hz, and a rat heart rate of 6.75 Hz) and

applied to three cases that produce the three characteristic behaviors. Since magnetic drug targeting localizes particles to a region by use of a magnet held locally for minutes, e.g. [4], but blood pulsation occurs once every second, it is appropriate to consider the averaged effect that the pulsating blood flow will have on particle concentration. Figure S4 shows the time averaged concentration profiles taken for three heart beats after a treatment window of one hour for the 9 chosen cases.

In comparison to [104], we do not consider a significant ferrofluid inlet concentration where the ferrofluid can then become an obstacle to the incoming flow and therefore we do not expect recirculation regions to be created. This phenomenon can make the average of the pulsatile case differ from the steady inlet flow case. Based on the range of biological parameters, the relevant non-dimensional numbers possible range between 0.01 (in capillaries) and 27 (in the largest vessels) for the Womersly number and the Reynolds number varies between 0.001 (in capillaries) and 3900 (in the largest vessels such as the aorta or vena cava).

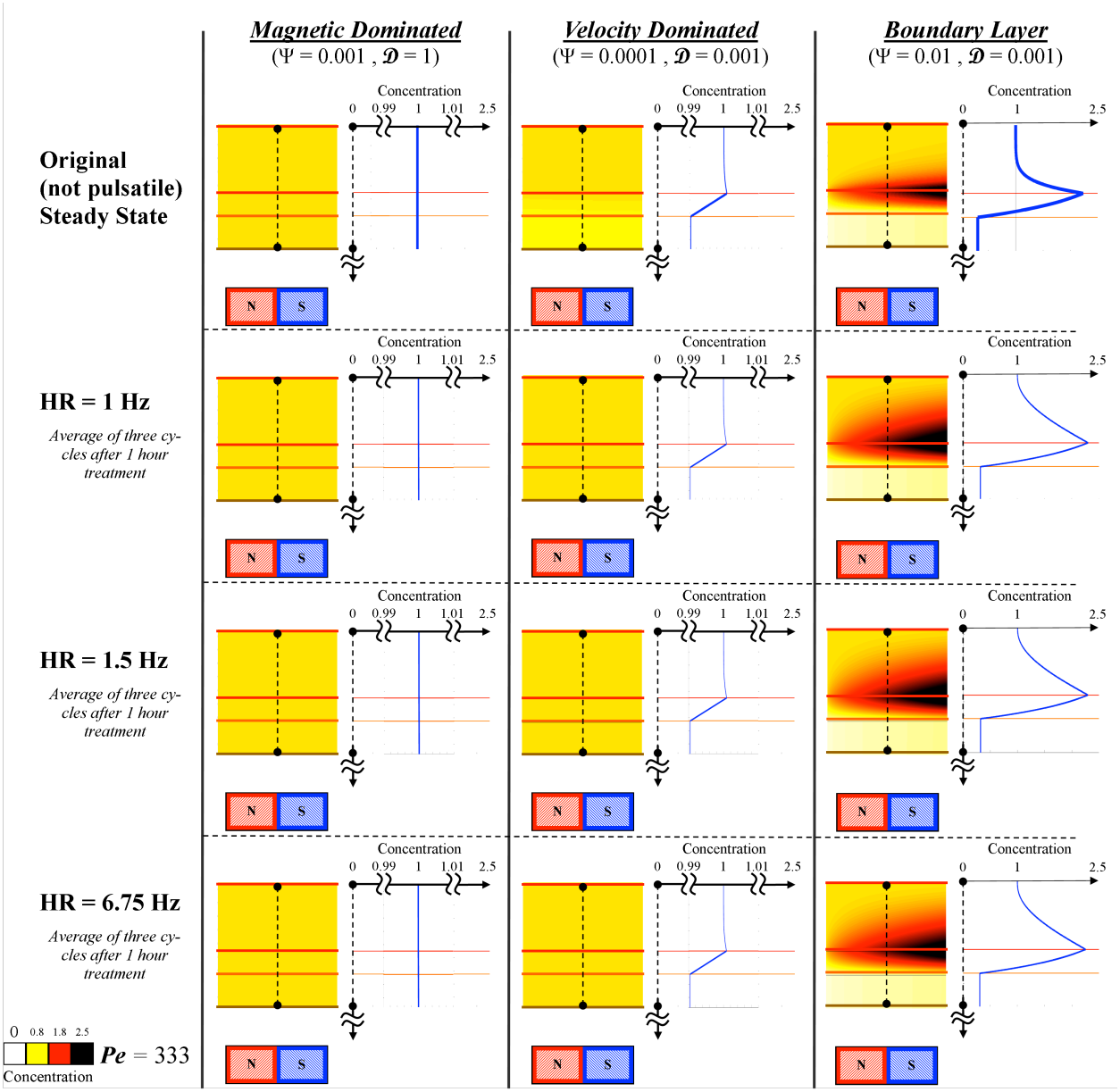

Figure S4: Pulsatile blood flow concentration profiles for the three characteristic behaviors experiencing three different heart rates (HR). For each pulsatile case, the concentration profile consists of the time average for three heart beats after a treatment window of one hour. This concentration can be compared to the prior steady state concentrations when blood flow pulsatility is not considered. The three behaviors are qualitatively the same and further are also similar quantitatively. (For this 333 Péclet number case, the Womersley and Reynold numbers can vary between 0.01 to 0.19 and 0.001 to 2.6 respectively for physiological and practical engineering conditions, according to the parameters in Table 1.)

Figure S4 shows that blood pulsatility under a uniform magnetic force field does not impact behavior delineation: the time-averaged concentration profiles remain in the magnetic dominated, velocity dominated, or boundary layer regime as they were in the constant blood flow case. This result has allowed for the simplification of the physiological model to the cycle-averaged blood velocity experienced within that vessel, a simplification we have used throughout the paper.

S3.3. Non-Uniform Magnetic Force Fields

In the main manuscript we treated the magnetic force as constant (see Figure 3). Here the exact magnetic field and the spatial variation in the resulting magnetic force on the magnetic particles is used. The magnetic force increases as the particles move closer to the magnet. Various parameters for a particular experiment will adjust how much the magnetic force increases in the blood vessel and surrounding tissue. These parameters include the size of the magnet, the size of the considered tissue-vessel system, and the distance of the tissue-vessel system from the magnet. In this section we exactly solve the magneto-static equations (1) to (3) and plug the computed magnetic field $\bar{H}(x,y)$ into equation (10) to state and solve the PDE for particle transport (previously the magnetic force $F \sim \nabla H^2$ was assumed to be a constant pointing downwards). To quantify the

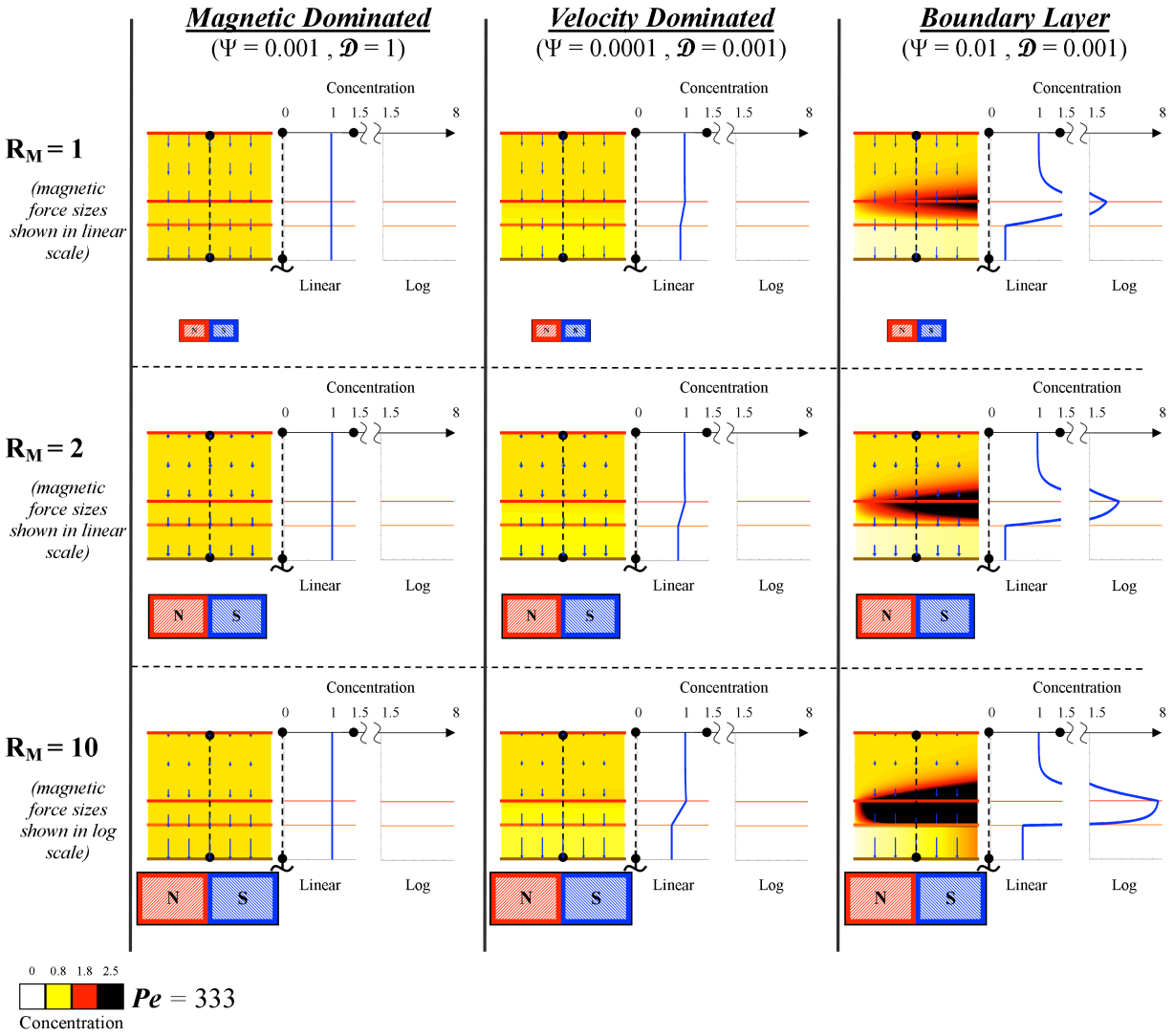

Figure S5: Concentration profiles for various magnetic force ratios. Three cases were chosen that illustrated the prototypical behaviors (magnetic dominated, velocity dominated, and boundary layer formation behavior) and the magnetic force ratio was changed from $\mathbf{R_M}$ = 1 to 2 and 10 by increasing the size of the magnet and reducing the distance between the vessel and magnet. The exact magnetic forces are shown as blue arrow overlays within each plot. The case of $\mathbf{R_M}$ = 1 and 2 show the arrow magnitudes in linear scale, while the case of $\mathbf{R_M}$ = 10 shows the arrow magnitudes in log scale (an arrow with twice the length will have ten times the magnitude).

deviation from a uniform magnetic force, we use the metric $R_M = F_{M,\max} / F_{M,centerline}$ where $F_{M,centerline}$ is the magnetic force along the blood vessel centerline and $F_{M,\max}$ is the maximum magnetic force within the considered vessel-tissue domain (it occurs at the bottom of the domain nearest the magnet corners where the magnetic field gradients are the highest). To examine how non-uniform magnetic force fields affect the three prototypical behaviors, three case studies were simulated for a varying magnetic force ratio of $\mathbf{R_M}$ = 2 and 10. $\mathbf{R_m}$ was varied by increasing the size of the magnet and reducing the distance between the vessel and magnet.

Figure S5 shows how the magnetic force ratio does not affect the prototypical behavior. When $\mathbf{R_M}$ = 1, the simulation is exactly equivalent to the cases considered in the main paper. As $\mathbf{R_M}$ increases, the maximum magnetic force at the bottom edge of the tissue-vessel system increases. In the case of a magnetic dominated behavior, the magnetic force ratio has very little to no effect on the solution. For velocity dominated cases, the vessel still maintains the inlet concentration value but the concentration in the tissue and membrane decreases due to increased pull from the magnet. Lastly, in the boundary layer formation cases, the vessel wall concentration simply increases. Since the vessel wall concentration at a given magnetic-Richardson number increases with the magnetic force ratio $\mathbf{R_m}$, the behavior delineation position (λ) will shift left in Figure 5 as the magnetic force ratio increases.

S3.4. Curved Blood Vessels

Blood vessels within any organism are rarely, if ever, straight. The idealized straight blood vessel used throughout the paper was relaxed and two different curvatures were utilized to determine the variance of the characteristic behaviors. The blood vessel length in each case was kept constant, and the only geometric parameter that changed was the radius of curvature. As can be seen in Figure S6 below, the characteristic behaviors retained their defining qualities. The only difference in cross-sectional concentration was seen in the boundary layer formation cases where the slight curvature case experienced a modest increase in concentration compared to no curvature or large curvature. This was because a slight curvature contained a longer segment of blood vessel in which the particles are able to form a boundary layer leading to a higher concentration build-up over that particular segment. However, this increase in concentration only shifts the boundary behavior delineation and does not change the overall observed behavior.

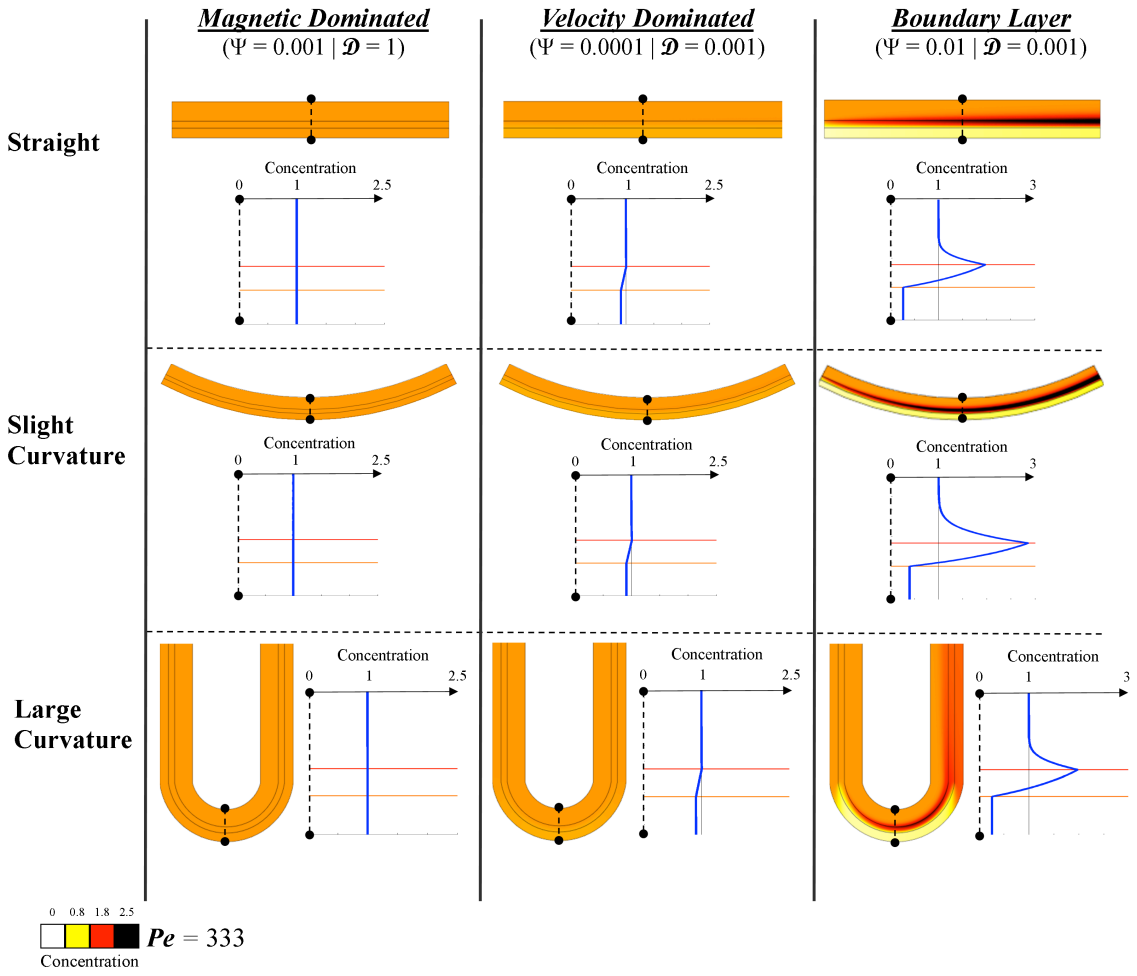

Figure S6: Curved blood vessels and the three prototypical behaviors. The curvature of the blood vessels does not affect the characteristic trend of the behaviors, but it can shift the behavior boundary delineation curve slightly.

S3.5. Particle Agglomeration

Agglomeration of particles can be considered approximately within our current framework. To do so, we think of a 'super-particle' composed of *n* ferro-magnetic particles stuck together. The magnetic force on such a particle increases by a factor of × *n*. However, the diameter of the particle goes only as $\sqrt[3]{n}$ since it takes 2 × 2 × 2 or × 8 particles to make a twice-as-big super-particle. Thus the Stokes drag force increases by $\sqrt[3]{n}$ and so the magnetic-Richardson number increases by $n^{2/3}$ (see equation (16)). For the nano-particles used in the rats of Figure 1b, if we consider a super-particle made up of 125 particles, the magnetic-Richardson number increases from 0.14 to 3.5. Since the super-particle has a larger radius, the blood and membrane diffusivities, D_B and D_M, will be smaller decreasing from 6 x 10^{-13} and 2 x 10^{-13} (for leaky capillaries with 600 nm pores) to 1 x 10^{-13} and 0 respectively. The scattering diffusion coefficient, D_S, will stay the same, however, since it is only dependent upon the type of blood vessel. This causes the mass Péclet number to increase from 1000 to 6000. The Renkin coefficient will instead decrease from 0.36 to 0. One can now read-off the behavior of such a particle from Figure 5 and 6 in the main paper as before: clearly, a case that was previously velocity dominated

could now fall into the boundary layer regime. In reality, during agglomeration there will be a statistical distribution of particle sizes, and chains can form instead of our simplified 'super particles'. To analyze such cases correctly requires additional research.

S3.6. Skin Boundary Condition

In animal and human trials, skin prevents magnetic particles from leaving the tissue. To model this case we enforce a boundary condition at the bottom of the tissue closest to the magnet that does not allow a flux of magnetic nano-particles across it. As expected, this causes a pile-up of particles just inside the skin nearest the magnet. Depending on the width of the tissue section being considered, this build-up can extend into the vessel region qualitatively distorting the three prototypical behaviors. Three case studies were chosen to examine the effect that the skin boundary has upon the solution.

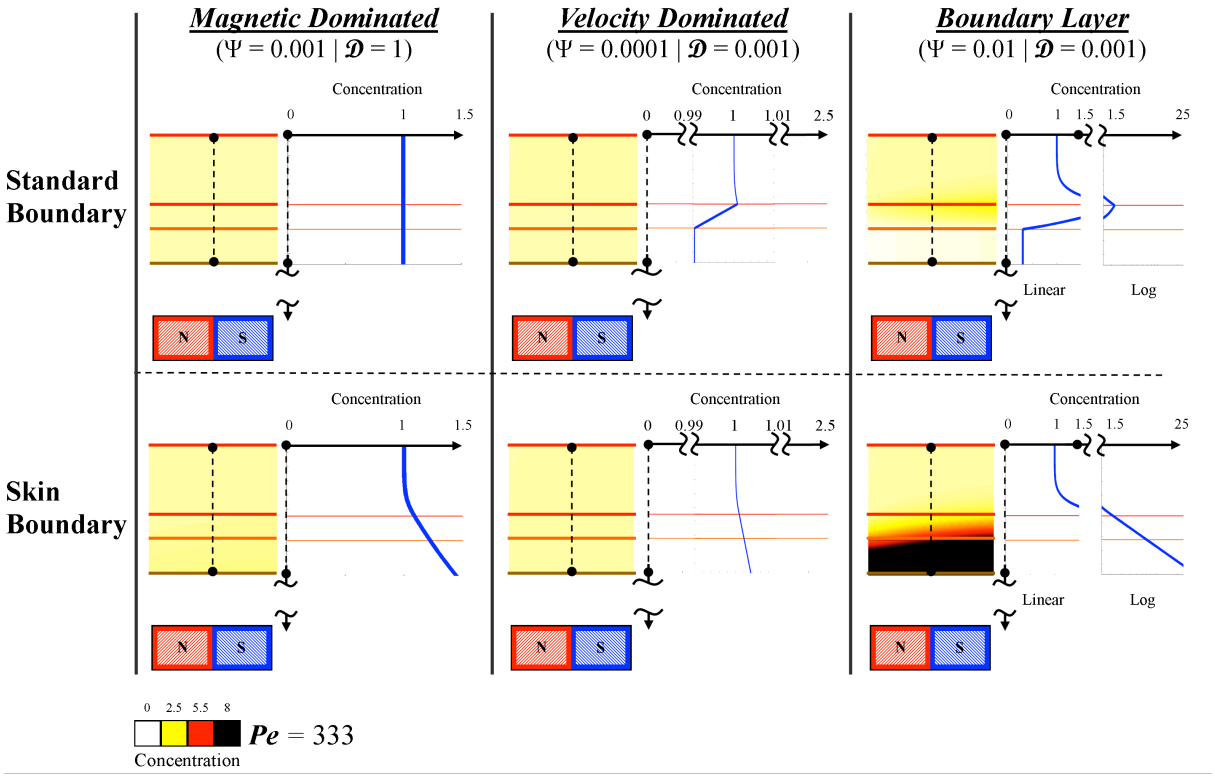

Figure S7: The effect that the skin boundary condition has upon the three prototypical behaviors can be seen by comparing the lower row to the top row of cases. The particles, once pulled through the vessel, travel to the skin boundary and then build-up along this interface and can extend back into the vessel region. This is most apparent in the magnetic dominated case where there is a build-up within the blood vessel membrane due to the presence of the skin boundary condition.

For any situation, if the blood vessel is close to the skin, the accumulation of ferrofluid at the skin can build up and can extend back through the tissue and into the vessel overwhelming any boundary layer that may otherwise have formed at the blood vessel wall. The magnetic dominated case saw an increase at the skin boundary, and a slight increase in particle concentration in the blood vessel due to the ability of the particles to build up at the skin. The velocity dominated case saw only a slight concentration build-up near the skin and a negligible change within the blood vessel. This is because particles are constantly washed out of the

vessel and not captured by the magnetic field thus they do not readily arrive at the skin interface. The boundary layer case had a significant increase in the particle concentration near the skin and vessel membrane, but very little change within the blood vessel. Particles in this case are pulled through the membrane and into the tissue with build-up near the skin only slightly affecting the blood vessel.

S3.7. Varying of Tissue Diffusivity

In the main text the Renkin tissue coefficient, $\mathcal{D}_{\mathcal{T}}$ (equation (20)), was always larger than the membrane Renkin coefficient, $\mathcal{D}$ (equation (18)), so that the limit to particle diffusion out of the vessel was the

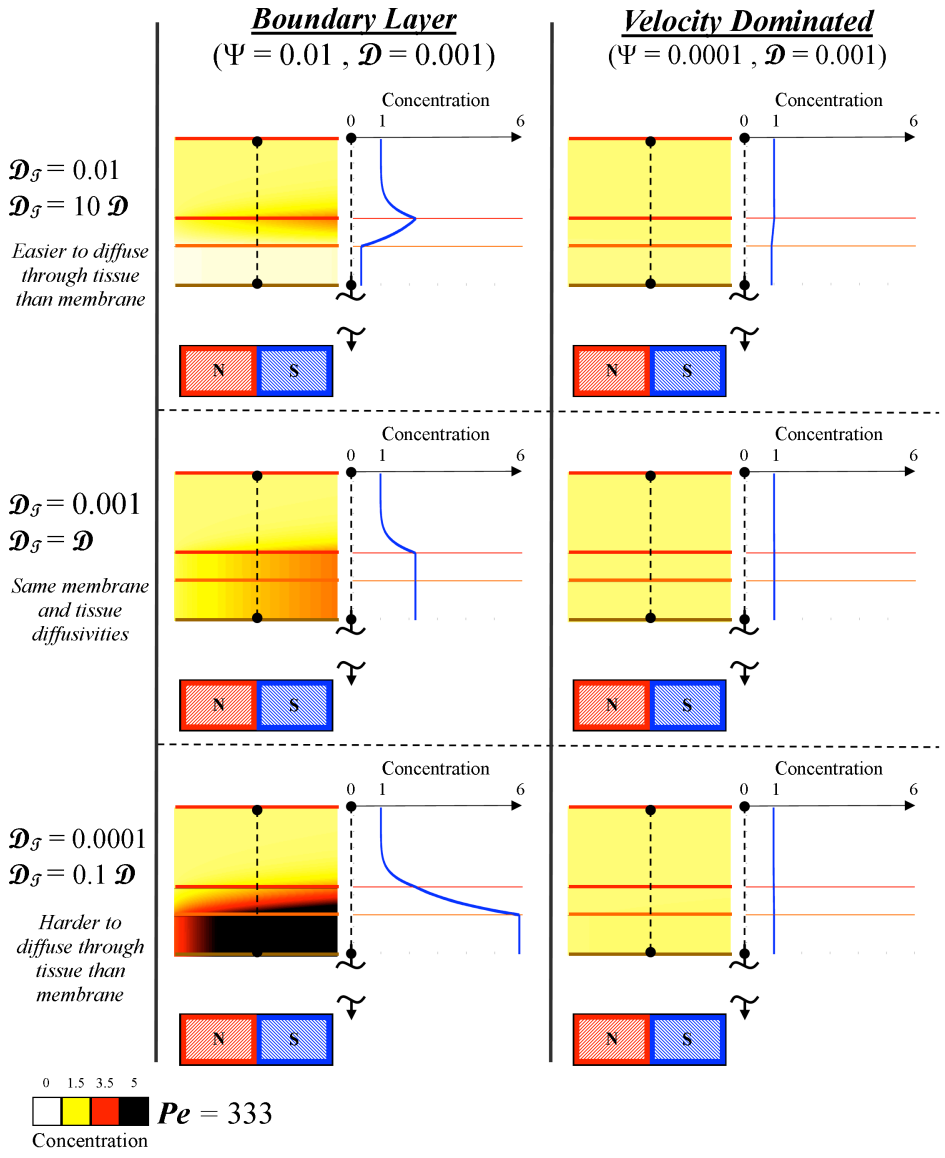

Figure S8: The effect on two prototypical behaviors by varying the Renkin reduced diffusion coefficent for tissue ($\mathcal{D}_{\mathcal{T}}$). The non-dimensional number cases used in the main text (Sections 4.2.2 and 4.2.3) are shown on the top row. The Renkin tissue coefficient is decreased in each subsequent row so that the membrane Renkin coefficient is the same as the Renkin tissue coefficient in the second row. The last row signifies a Renkin tissue coefficient an order of magnitude less than the membrane Renkin coefficient.

membrane. This behavior is consistent with many tissue-vessel systems but not all [31]. There are physiological conditions were the underlying tissue might not allow diffusion of particles as easily as a membrane, the Renkin tissue coefficient would then be smaller than the membrane Renkin coefficient. Therefore the effect on particle concentration for changing the Renkin tissue coefficient (a fourth non-dimensional number) must be examined. Two cases were chosen to explore the effect changing tissue diffusivity has upon the steady-state concentration: boundary layer formation and velocity dominated behavior. Since the magnetic dominated behavior occurs only at Renkin reduced diffusion coefficients that are near unity, it does not make sense to vary the tissue diffusivity significantly for a magnetic dominated case.

The above figure shows cases where the Renkin reduced diffusion coefficient for the tissue is changed while the regular (endothelial membrane) Renkin reduced diffusion coefficient is held constant at $\mathcal{D}$ = 0.001. The first row ($\mathcal{D}_{\mathcal{T}}$ = 0.01) corresponds to the typical cases used in this paper where we have assumed that diffusion in the tissue is x 10 greater than the diffusion in the endothelium (diffusion in the tissue is 1/100th that of blood while diffusion in the membrane is 1/1000th that of blood). The second row ($\mathcal{D}_{\mathcal{T}}$ = 0.001) shows the concentration if the two Renkin values are equal (diffusion in the both tissue and membrane is 1/1000th that of blood). Here it is possible to see that the tissue space becomes an extension of the membrane space with an equivalent behavior (because $\mathcal{D}_{\mathcal{T}} = \mathcal{D}$). The third row ($\mathcal{D}_{\mathcal{T}}$ = 10^{-4}) shows the solution when the diffusion in the tissue is x 10 smaller than the diffusion in the endothelium (diffusion in the tissue is 1/10000th that of blood while diffusion in the membrane is 1/1000th that of blood). Now the tissue space holds the primary concentration of particles. In all cases, the steady state vessel wall concentration remains essentially constant as we change the tissue Renkin value. This suggests that the relationship between these two Renkin values merely effects the distribution of particles between the membrane and the tissue and not the vessel concentration. Since the vessel wall concentration is not easily effected, the three prototypical behaviors and their delineation boundaries do not change.

S3.8. Different Particle Hydrodynamic and Magnetic Core Radii

For simplicity, typically the hydrodynamic and magnetic core radii are assumed to be equal. Most often this is not exactly the case and there is a slight mismatch between the two values due to particle coatings that are added onto either affix therapeutics or immune system evading mechanisms [7, 9]. Then the hydrodynamic radius is slightly larger than the magnetic core radius leading to an increase in the Stokes drag force compared to the magnetic force. In this case, equation (4) would remain the same and equations (6) and (7) would change to

(S8) $$\vec{F}_S = 6\pi r \eta \vec{V}_R$$

(S9) $$\vec{V}_R = \frac{a^3}{9\eta r}\frac{\mu_0 \chi}{(1+\chi/3)}\nabla\left(\left|\vec{H}\right|^2\right)$$

where r is the hydrodynamic radius of a particle. Therefore the non-dimensional magnetic-Richardson number changes in addition to a slight change in the Péclet and Renkin numbers. Using the same rat example as throughout the paper, if the 250 nm diameter particle had a 300 nm hydrodynamic diameter, the magnetic force acting upon this particle would remain constant while the Stokes drag force changes from 0.70 pN to 0.84 pN. This would cause a slight decrease in the magnetic-Richardson number from 0.14 to 0.12. Since the

particle has a larger radius, the blood and membrane diffusivities, D_B and D_M, will be smaller decreasing from 6 x 10^{-13} and 2 x 10^{-13} (for leaky capillaries with 600 nm pores) to 5 x 10^{-13} and 1.4 x 10^{-13} respectively. The scattering diffusion coefficient, D_S, will stay the same, however, since it is only dependent upon the type of blood vessel. This causes the mass Péclet number to increase from 1000 to 1200. The Renkin coefficient will instead decrease from 0.36 to 0.28.

S3.9. Non-Perpendicular Magnetic Force

For blood vessels in animal or human vasculature, the alignment of the blood vessels obviously varies and the applied magnetic force may not be perpendicular to the blood flow. We considered this case in the main text because it is the least complex scenario to think about, and because it represents a best case (the magnetic force is lined up to extract as many particles as possible). A simple first approximation of the ferrofluid behavior for the case when a blood vessel is not aligned perpendicular to the magnet force is to separate the magnetic force into the perpendicular (*y*-direction in Figure 2) and parallel (*x*-direction in Figure 2) components. Then the perpendicular magnetic force component can be used as the magnetic force in equation (16), while the parallel component can be added to the Stokes drag force to be used as a 'net' Stokes drag force in equation (16) to compute a modified magnetic-Richardson number that takes into account the magnetic force misalignment.

S4. Determination of Experimental Domains

In-vivo experiments often contain a wide range of physical variables that fold into the development of the three non-dimensional numbers. These numbers are dictated by the biology of the system studied and include items such as varying blood vessel widths, blood vessel velocities, and diffusion coefficients within various tissues, membranes, and blood vessels. Typically information is not known about the exact physical variables experienced by every nano-particle within the animal or human at any specific time. Some particles can be within liver regions, while others are floating within skin tissue. Therefore, the anaalysis of the entire biological system must include educated estimates for the expected range of all the key non-dimensional numbers. Our three non-dimensional numbers are written again below with the biologically varying parameters marked by a double underline:

$$\text{(S10)}\quad \Psi = \frac{\text{Magnetic Force at Centerline}}{\text{Stokes Drag Force at Centerline}} = \left|\frac{\vec{F}_M}{\vec{F}_S}\right| = \frac{6\pi a\eta\, k\,\nabla\left(\left|\vec{H}\right|^2\right)}{6\pi a\eta\, \underline{\underline{V_{B\max}}}} = \frac{\vec{V}_R}{\underline{\underline{V_{B\max}}}}$$

$$\text{(S11)}\quad \boldsymbol{Pe} = \frac{\text{Blood Vessel Width} \times \text{Maximum Blood Velocity}}{\text{Total Diffusion Coefficient of Particles}} = \frac{\underline{\underline{d_B}}\,\underline{\underline{V_{B\max}}}}{D_B + \underline{\underline{D_S}}}$$

$$\text{(S12)}\quad \mathcal{D} = \frac{\text{Minimum Diffusion Coefficient in Membrane or Tissue}}{\text{Total Diffusion Coefficient in Blood}} = \frac{\min(\underline{\underline{D_M}}, \underline{\underline{D_T}})}{D_B + \underline{\underline{D_S}}}$$

S4.1. Magnetic-Richardson Number Range

As shown in equation (S10), the magnetic-Richardson number is only dependent upon one biological variable: the centerline blood velocity. Therefore the range of the magnetic-Richardson number is as follows

(S13) $$\frac{\vec{V}_R}{V_{B\max}\big|_{\max}} \le \Psi \le \frac{\vec{V}_R}{V_{B\max}\big|_{\min}}$$

where $V_{B\max}$ is the centerline (maximum) velocity in the blood vessel and $\big|_{\max}$ and $\big|_{\min}$ denote the maximum and minimum of this velocity across physiological conditions, at major veins versus capillaries respectively.

S4.2. Renkin Reduced Diffusion Coefficient Range

Equation (S12) illustrates the fact that the Renkin reduced diffusion coefficient is dependent upon the diffusion in the membrane, the diffusion in the tissue, and the scattering diffusion coefficient due to blood vessel size and velocity. The tissue and membrane diffusion coefficients are properties of the tissue and can range from a lower bound of 'zero' when the particle is larger than the membrane pores or tissue interstitial spaces, to an upper bound equal to the diffusion coefficient within the blood. The scattering diffusion coefficient can be estimated by using the following formula [69]

(S14) $$D_S \approx K_{sh}\,(r_{RBC})^2\,\dot{\gamma} \approx 8K_{sh}\,(r_{RBC})^2\,\frac{V_{B\max}}{d_B}$$

where the dimensionless coefficient is $K_{sh} = 5\times10^{-2}$, the red blood cell radius is $r_{RBC} = 4.26\times10^{-6}$ m, and $\dot{\gamma}$ is the shear rate at the vessel wall. Therefore the range for all Renkin reduced diffusion coefficients is

(S15) $$\frac{\min(D_M\big|_{\min}, D_T\big|_{\min})}{D_B + D_S\big|_{\max}} \le \mathcal{D} \le \frac{\min(D_M\big|_{\max}, D_T\big|_{\max})}{D_B + D_S\big|_{\min}}$$

S4.3. Mass Péclet Number Range

The mass Péclet number varies with more complexity than the other two numbers as is evident from equation (S11). The numerator varies not only with the centerline velocity of a vessel but also with the diameter of that vessel. Physiologically the velocity is also dependant upon the diameter of the vessel and the exact shape of this dependency is not linear. In addition the denominator is also dictated by the scattering diffusion coefficient that is governed by the vessel diameter. From equations (S11) and (S14), the needed dependencies and bounds on the Péclet number are

(S16) $$\boldsymbol{Pe} = \frac{d_B\left(V_{B\max}\right)\times V_{B\max}}{D_B + D_S\left(V_{B\max}\right)}$$

(S17) $$\frac{d_{B\min}\left(V_{B\max}\big|_{\min}\right)\times V_{B\max}\big|_{\min}}{D_B + 8K_{sh}\,(r_{RBC})^2\,\dfrac{V_{B\max}\big|_{\max}}{d_{B\min}\left(V_{B\max}\big|_{\min}\right)}} \le \boldsymbol{Pe} \le \frac{d_{B\max}\left(V_{B\max}\big|_{\max}\right)\times V_{B\max}\big|_{\max}}{D_B + 8K_{sh}\,(r_{RBC})^2\,\dfrac{V_{B\max}\big|_{\min}}{d_{B\max}\left(V_{B\max}\big|_{\max}\right)}}$$

To understand the shape of the mass Péclet curve, the relationship between the vessel diameter and centerline blood velocities must be known or estimated. For some organisms, i.e. humans, this relationship is well known [1] and appropriate bounds for these data points can be determined. For other organisms, i.e. rats, the relationship is not well known and bounds must be estimated more roughly to allow all possibilities. Figure

S9 shows the relationship within humans for the vessel diameter to the vessel velocity [1] with our two chosen bounding curves for the data shown.

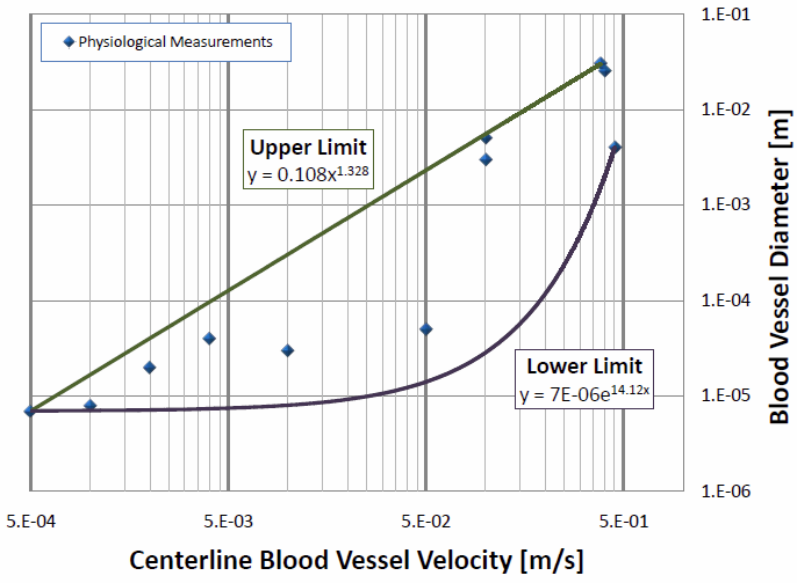

Figure S9: Relationship between vessel diameter and blood vessel velocity within humans [1]. Our chosen upper and lower limits to bound the data are shown.

The combination of these ranges for the non-dimensional numbers generates the shape of the experimental domains seen in Figure 11 of the main text. These domains are simple (conservative) rectangles when only general physiological information is known (Bergemann, Widder), they are tighter curved domains for the situation in humans (Lubbe) where more specific physiological information is available.